A Novel Grid-Connected Photovoltaic Centralized Inverter Topology to Improve the Power Harvest during Partial Shading Condition

REFAAT A., ELGAMAL M., KOROVKIN N.V.

Grid-connected centralized inverters based on traditional topologies are one of the best solutions for medium and large-scale photovoltaic (PV) power plants due to their low cost and simplicity. However, the output power of these conventional topologies is drastically decreased because of partial shading effects or mismatch between PV panels. This paper proposes a new grid-connected centralized inverter topology based on a novel photovoltaic current collector optimizer (CCO) to enhance the power yield from PV array in case of partial shading or PV modules mismatch. The PV modules are stacked by CCOs and then interfaced to the grid through three phase-two level voltage source inverter (VSI). The CCOs are used to improve the power harvest from PV array instead of using bypass and blocking diodes which deforms the PV array characteristics and reduces its output power. The VSI is used to inject a high-quality AC current into the grid and perform maximum power point tracking (MPPT) together. Computer simulation is carried out using MATLAB/Simulink in order to test operation of the proposed topology. Simulation results show that the proposed topology offers an excellent steady-state response, fast dynamic response, perfect and robust tracking of maximum power point during partial shading condition.

K e y   w o r d s: *photovoltaic system, current collector optimizer (CCO), grid-connected centralized inverter topologies, P&O MPPT, current control VSI, power quality, efficiency, partial shading*

I. INTRODUCTION

Over recent years, the problems of energy shortage and environmental contamination have become critical research topics worldwide. Thus, the trends of employing distributed generation systems (DGSs) based on renewable energy are drawing more and more attention for reducing energy crisis and carbon emission. Among all various DGSs, solar photovoltaic (PV) systems are rapidly growing in electricity markets and are expected to continue this trend throughout the near future. Nevertheless, the unit cost of energy obtained from PV systems is still high compared to traditional energy sources and other forms of renewables; accordingly, current research focuses on decreasing manufacturing costs and increasing the energy production of the overall PV systems [1], [2].

On the basis of the different arrangements of PV modules, the grid-tied PV inverter technologies can be classified into central inverters, string inverters, multistring inverters, and AC-module inverters or micro-inverters. Central inverter technology is the most common topologies of PV installation, which interfaced a large number of panels that configured in series-parallel (SP) combination to the grid. The main technical challenge for central inverter technology is the absence of a maximum power point operation for each module due to partial shading as well as bypass diodes that is used to prevent modules from hotspot effect deforms the PV array characteristics and exhibits multiple peaks, including a global and local maximum power points. That force researchers to look for different technologies for the interconnections of the PV modules [3], [4].

The most typical solutions to partial shading effects and mismatch conditions are AC-module inverters, which utilize micro-inverters/converters for each individual PV module to adopt distributed MPPT (DMPPT). All PV modules have the ability to be operated at each maximum power point (MPP), even under partial shading or mismatch conditions, because of the individual control for each module which improves the power efficiency of PV system. The major disadvantages of AC-module inverters are high cost and increased system complexity since the number of micro-inverters/converters is proportional to that of PV modules [4], [5].

Other solutions to eliminate local MPPs and increase maximum available power are using differential power processing (DPP) converters and voltage or current equalizers. With DPP converters or equalizers, a portion of the generated power of unshaded modules is transferred to shade ones thus all the modules operate at the same voltage or even at each MPP. Several types of DPP converters and equalizers have been proposed and developed in literatures [5–16]. Generally, a switch count in a converter can show a good hint about system complexity due to each switch requires a gate drive controller circuit and comprising its individual electronic components.

Besides the system efficiency, high-quality injected power is another essential feature of grid-connected PV (GCPV) systems. The quality of injected power is mainly governed by practices and standards on voltage, frequency, and harmonics. In particular, GCPV systems should have low current harmonic distortion to assure that no adverse effects are caused to other equipment connected to the utility grid. IEEE standard 929 for utility interface of PV systems recommended that most PV inverters designed for utility-interconnected service operate close to unity power factor with total harmonic current distortion not more than 5% at rated inverter power output[17], [18].

This paper aims at evaluating the performance of 100 kW GCPV system by using a new centralized inverter topology based on a novel photovoltaic current collector optimizer (CCO). The main objectives are to improve the power extracted from PV array during partial shading condition, avoid the misleading power loss due to local MPPs, eliminate the power loss associated with circulating currents between parallel PV generators, and inject a high quality AC current into the grid to meet the standard IEEE 929.

II. SYSTEM DESCRIPTION

The schematic diagram of the proposed grid-tied centralized inverter based on current collector optimizer (CCO) is depicted in figure 1. The power circuit consists of a 100 KW PV array with CCOs, DC-link capacitor, three phase-two level voltage source inverter (VSI), LC filter, low-frequency step-up transformer, and grid. The utility grid is modeled by

Thevenin equivalent circuit as a three-phase voltage source and series impedances, while the PV module is represented by a single exponential model (aka one diode model) as described in the literature [18]. As can be seen in the diagram, every eight modules or substrings are connected to CCO as a single stack and then these stacks may be connected in series-parallel combination to the grid through an inverter. For control schemes, two control circuits are employed for the grid-connected centralized inverter. The first control circuit regulates the H-bridges of the CCOs to enhance the output power of the PV array under partial shading condition, which is not shown in the diagram. The second control circuit regulates the VSI to extract maximum power from CCOs as well as controls the current injected into the grid to meet the standard IEEE 929.

A. Control of Current Collector Optimizer (CCO)

The main idea of the current collector optimizer (CCO) is to find a way to harvest the currents from PV modules or substrings at approximately maximum power point (MPP) voltages during shading condition. Hence, there is no need for the shaded module or substring to be short-circuited through bypass diodes. The circuit diagram of the CCO is as shown in figure 2. This circuit is a modified circuit that is used to collect the current from magnetohydrodynamic generator electrodes' which have different voltages and it can be found in the literature [19].

As depicted in Figure 2, all PV generators negative terminals' are connected to a common negative line while each positive terminal is connected to
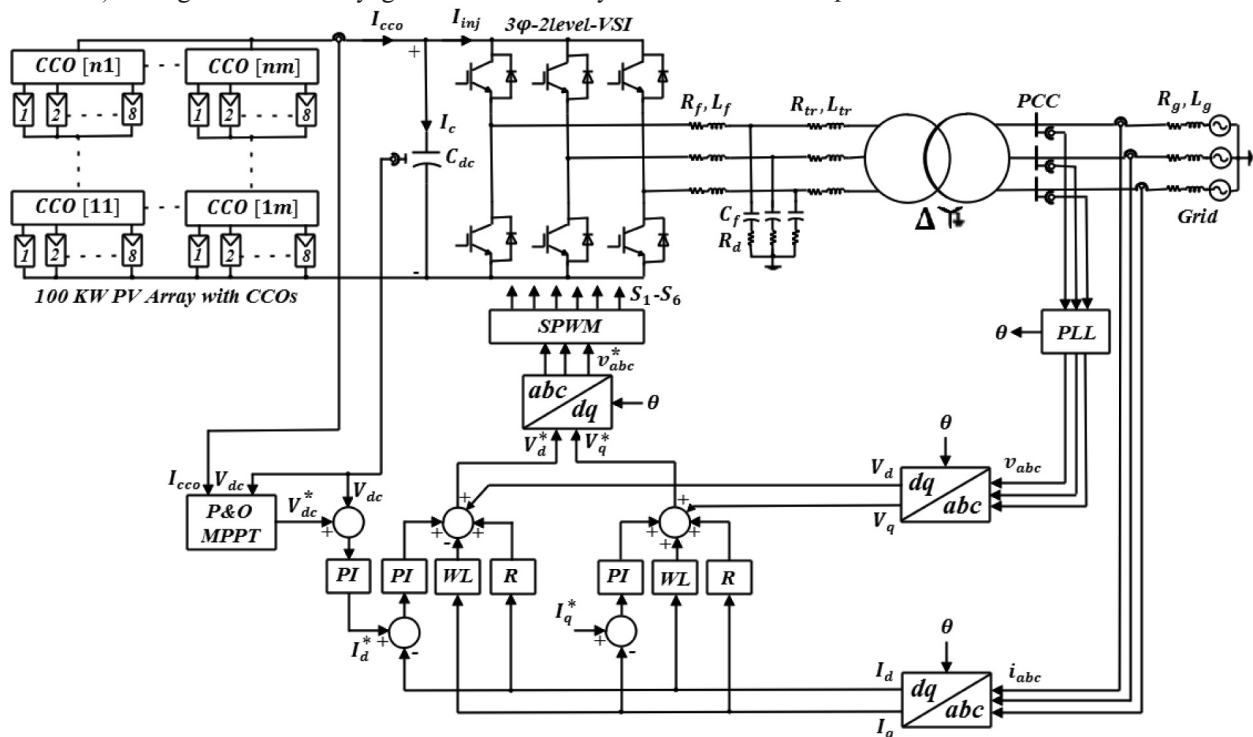
Figure 1. The schematic diagram of the proposed topology
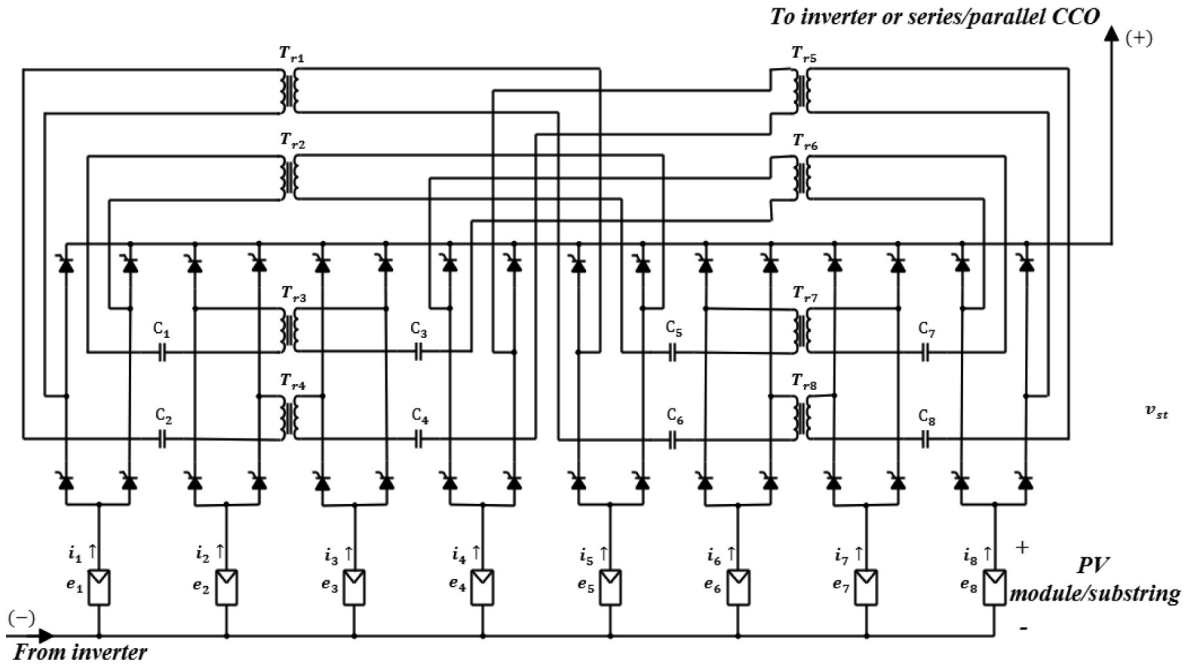
Figure 2. Circuit diagram of the CCO

thyristor-bridge and then all bridges are gathered in common positive line. The H-bridges are interconnected with each other through eight capacitors ($C_1 - C_8$) and transformers ($Tr_1 - Tr_8$) which act as self-commutation circuit and compensate the voltage difference between parallel PV generators. The bridge thyristors' are controlled so that at first half cycle two diagonally opposite thyristor $T_1 \& T_4$ are forward biased while the other two thyristors $T_2 \& T_3$ are reversed biased and vice versa at the second half cycle. Therefore, the upper and lower capacitors between adjacent PV generators alternatively change their polarities every half cycle. Forced commutation of thyristors is carried out during discharge of coupling condensers. Figure 3 shows the voltage waveforms across upper and lower capacitors and the
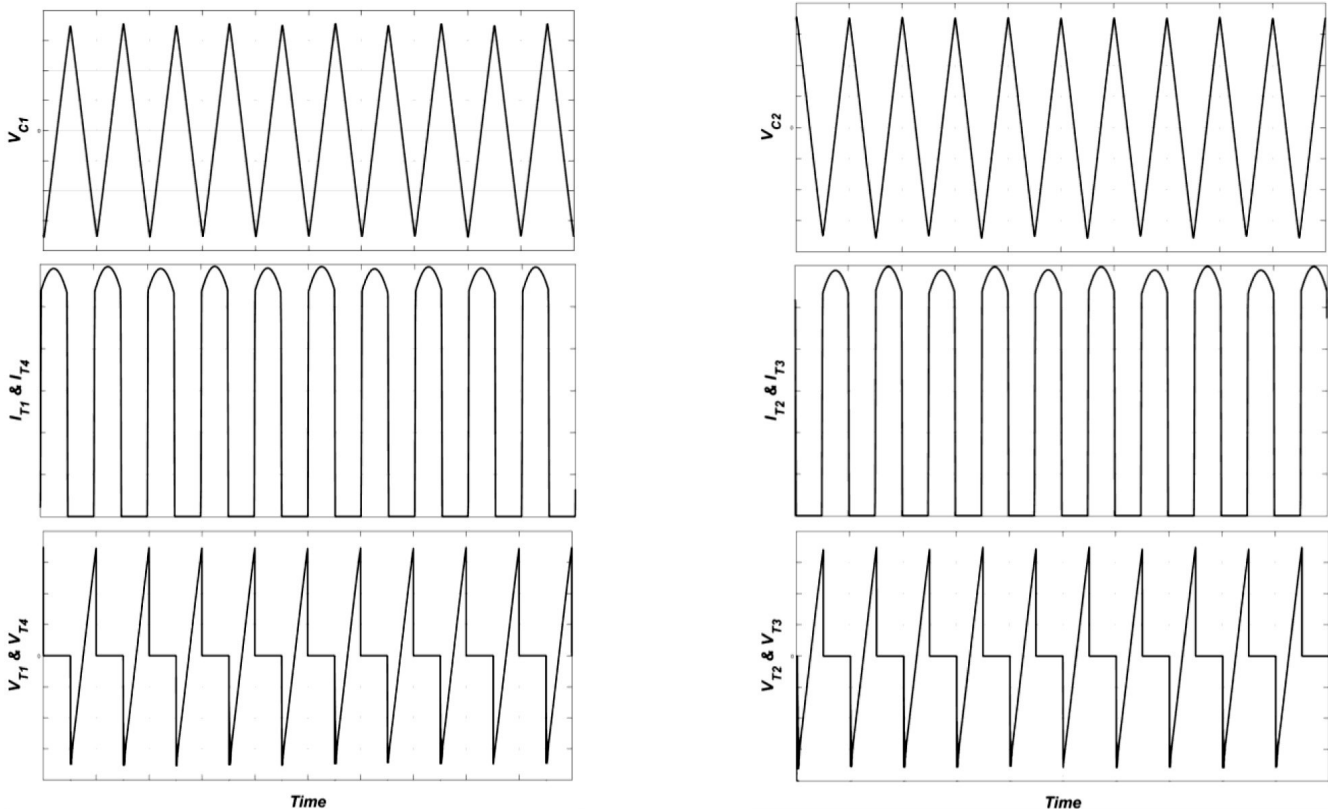
Figure 3. The voltage across condensers and the corresponding current and voltage waveforms of the SCRs

corresponding current and voltage waveforms of the SCRs during steady-state operation of the CCO.

The coupling transformers are symmetrically linked to each other concerning the power production section center. Their function is to compensate the voltage difference between PV modules; under shading condition, to a current consolidation point v_{st}. The transforms are represented by inductances and mutual coupling with approximately unity coupling factor (k) as given below.

$$R_m = k\sqrt{R_{s1}R_{s2}}; \tag{1}$$

$$L_m = k\sqrt{L_{s1}L_{s2}} \quad \& \quad 0 \leqslant k \leqslant 1. \tag{2}$$

Where $R_{s1}\,\&\,R_{s2}$ are the self-resistance of primary and secondary windings, $L_{s1}\,\&\,L_{s2}$ are self-inductance of primary and secondary windings, $R_m\,\&\,L_m$ are mutual resistance and inductance of the transformer.

In the first half cycle, the current and voltage equations of a single stack CCO are as follows:

$$e_1 - 2R_s i_1 - 2L_s\frac{di_1}{dt} - R_m i_3 - L_m\frac{di_3}{dt} - R_m i_5 -$$
$$- L_m\frac{di_5}{dt} - v_{C1} - v_{st,i} = 0; \tag{3}$$

$$e_2 - 2R_s i_2 - 2L_s\frac{di_2}{dt} - R_m i_4 - L_m\frac{di_4}{dt} - R_m i_6 -$$
$$- L_m\frac{di_6}{dt} - v_{C2} - v_{st,i} = 0; \tag{4}$$

$$e_3 - 2R_s i_3 - 2L_s\frac{di_3}{dt} - R_m i_1 - L_m\frac{di_1}{dt} - R_m i_7 -$$
$$- L_m\frac{di_7}{dt} - v_{C3} - v_{st,i} = 0; \tag{5}$$

$$e_4 - 2R_s i_4 - 2L_s\frac{di_4}{dt} - R_m i_2 - L_m\frac{di_2}{dt} - R_m i_8 -$$
$$- L_m\frac{di_8}{dt} - v_{C4} - v_{st,i} = 0; \tag{6}$$

$$e_5 - 2R_s i_5 - 2L_s\frac{di_5}{dt} - R_m i_1 - L_m\frac{di_1}{dt} - R_m i_7 -$$
$$- L_m\frac{di_7}{dt} - v_{C5} - v_{st,i} = 0; \tag{7}$$

$$e_6 - 2R_s i_6 - 2L_s\frac{di_6}{dt} - R_m i_2 - L_m\frac{di_2}{dt} - R_m i_8 -$$
$$- L_m\frac{di_8}{dt} - v_{C6} - v_{st,i} = 0; \tag{8}$$

$$e_7 - 2R_s i_7 - 2L_s\frac{di_7}{dt} - R_m i_3 - L_m\frac{di_3}{dt} - R_m i_5 -$$
$$- L_m\frac{di_5}{dt} - v_{C7} - v_{st,i} = 0; \tag{9}$$

$$e_8 - 2R_s i_8 - 2L_s\frac{di_8}{dt} - R_m i_4 - L_m\frac{di_4}{dt} - R_m i_6 -$$
$$- L_m\frac{di_6}{dt} - v_{C8} - v_{st,i} = 0; \tag{10}$$

$$i_{st,r} = \sum_{j=1}^{8} i_j. \tag{11}$$

Where $i_{st,r}$ is the stack current, $v_{st,i}$ is the stack voltage, i_j are the currents generated by PV modules, e_j are PV modules voltages and the voltage across coupling capacitors.

In the second half cycle,

$$e_1 - 2R_s i_1 - 2L_s\frac{di_1}{dt} - R_m i_3 - L_m\frac{di_3}{dt} - R_m i_5 -$$
$$- L_m\frac{di_5}{dt} - v_{C2} - v_{st,i} = 0; \tag{12}$$

$$e_2 - 2R_s i_2 - 2L_s\frac{di_2}{dt} - R_m i_4 - L_m\frac{di_4}{dt} - R_m i_6 -$$
$$- L_m\frac{di_6}{dt} - v_{C1} - v_{st,i} = 0; \tag{13}$$

$$e_3 - 2R_s i_3 - 2L_s\frac{di_3}{dt} - R_m i_1 - L_m\frac{di_1}{dt} - R_m i_7 -$$
$$- L_m\frac{di_7}{dt} - v_{C4} - v_{st,i} = 0; \tag{14}$$

$$e_4 - 2R_s i_4 - 2L_s\frac{di_4}{dt} - R_m i_2 - L_m\frac{di_2}{dt} - R_m i_8 -$$
$$- L_m\frac{di_8}{dt} - v_{C3} - v_{st,i} = 0; \tag{15}$$

$$e_5 - 2R_s i_5 - 2L_s\frac{di_5}{dt} - R_m i_1 - L_m\frac{di_1}{dt} - R_m i_7 -$$
$$- L_m\frac{di_7}{dt} - v_{C6} - v_{st,i} = 0; \tag{16}$$

$$e_6 - 2R_s i_6 - 2L_s\frac{di_6}{dt} - R_m i_2 - L_m\frac{di_2}{dt} - R_m i_8 -$$
$$- L_m\frac{di_8}{dt} - v_{C5} - v_{st,i} = 0; \tag{17}$$

$$e_7 - 2R_s i_7 - 2L_s\frac{di_7}{dt} - R_m i_3 - L_m\frac{di_3}{dt} - R_m i_5 -$$
$$- L_m\frac{di_5}{dt} - v_{C8} - v_{st,i} = 0; \tag{18}$$

$$e_8 - 2R_s i_8 - 2L_s\frac{di_8}{dt} - R_m i_4 - L_m\frac{di_4}{dt} - R_m i_6 -$$
$$- L_m\frac{di_6}{dt} - v_{C7} - v_{st,i} = 0. \tag{19}$$

The overall circuit current, voltage and power are given by the following equations:

$$V_{dc} = \sum_{i=1}^{n} v_{st,i}; \qquad (20)$$

$$I_{CCO} = \sum_{r=1}^{m} i_{st,r}; \qquad (21)$$

$$P_{dc} = V_{dc} I_{CCO}. \qquad (22)$$

Where n and m are the number of stacks connected in series and parallel respectively.

B. Control of Voltage Source Inverter (VSI)

A current controlled sinusoidal PWM (SPWM) technique is used to control the VSI in *d-q* synchronous reference frame (SRF). The main target of the control strategy is to regulate the inverter output current to follow a specified reference signal. This technique includes multi loops control. The outer loop regulates the DC link voltage to track the MPP voltage of the CCOs, while the inner loops control the direct and quadrature currents that aligned the grid voltage vector. The phase-locked loop (PLL) is used to extract the grid voltage vector angle (θ).

In order to determine the MPP voltage of the CCOs, the DC link reference voltage (V_{dc}^*) is adjusted by using perturb and observe (*P&O*) MPPT technique. The flowchart of the *P&O* MPPT algorithm is as shown in figure 4. The PI controller output of the DC link voltage dynamics is used as the reference of direct current component (I_d^*). The reference command direct current can be written as:

$$I_d^* = K_p(V_{dc}^* - V_{dc}) + K_I \int (V_{dc}^* - V_{dc})dt. \qquad (23)$$

Where K_p and K_I are the PI controller parameters.

It is worth mentioning that, the low-frequency step-up transformer can contribute in harmonics filtering, where *LCL* filter is formed if the leakage inductance of the transformer is referred to primary side (PV array side). The line *LCL* filter is designed according to reference [20].

To design the inner loops controller it is recommended to neglect the filter capacitor using the *L* approximation of the *LCL* filter [21]. This is possible because the low frequency behavior of the *LCL* filter is similar to an *L* filter as can be seen in figure 5.

At point of common coupling (PCC), the voltage and current vectors are measured and transformed in *d-q* reference frame. By adopting decoupled control, the command voltage equations by the inverter in *d-q* reference frame can be described as:

$$\begin{cases} V_d^* = RI_d + V_d - wLI_q + K_p(I_d^* - I_d) + \\ + K_I \int (I_d^* - I_d)dt; \\ V_q^* = RI_q + V_q + wLI_q + K_p(I_q^* - I_q) + \\ + K_I \int (I_q^* - I_q)dt. \end{cases} \qquad (24)$$
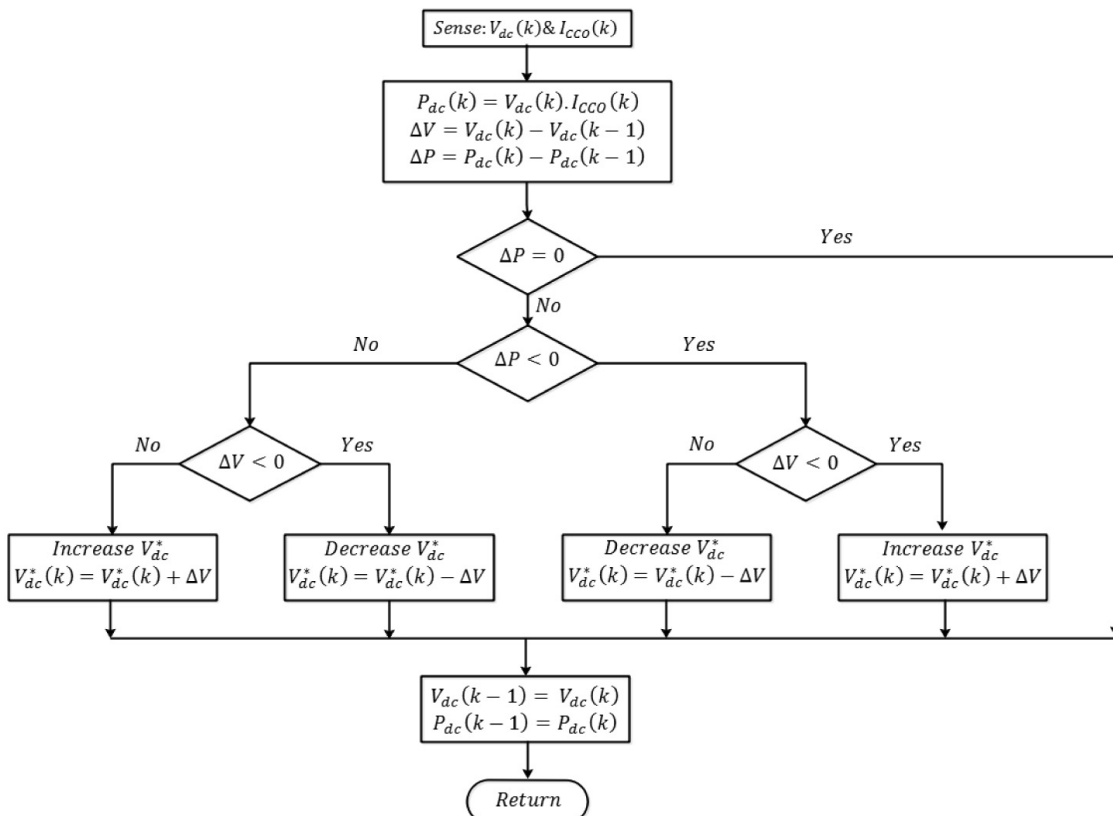
Figure 4. The flowchart of the *P&O* algorithm
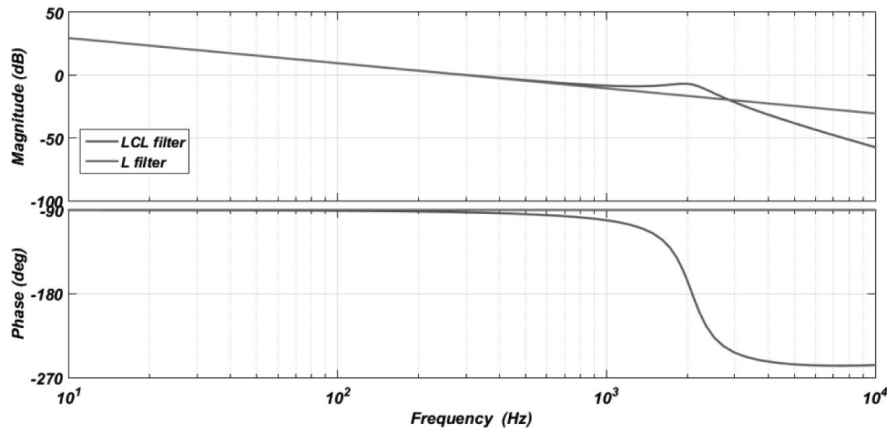
Figure 5. Bode diagram of line filters

Where V_d^* and V_q^* are the *d-q* reference voltages, V_d and V_q are the *d-q* voltages at PCC, I_d and I_q are the *d-q* currents, $(R = R_f + R_{tr})$ is the equivalent resistance of the control loop, $(L = L_f + L_{tr})$ is the equivalent inductance of the control loop, R_f and L_f are the filter resistance and inductance, R_{tr} and L_{tr} are the transformer resistance and inductance referred to primary side.

In order to control the active and reactive power injected in the grid, the PLL is adjusted so the *q*-axis component of the grid voltage vector (V_q) equal to zero. The power equations can be written as:

$$\begin{cases} P = V_d I_d; \\ Q = -V_d I_q. \end{cases} \qquad (25)$$

Thus, the active and reactive power can be controlled independently by controlling the direct and quadrature current. For unity power factor, it is required to force the reactive power to zero, thus the reference command quadrature current (I_q^*) is set to zero. Finally, the command voltages are transformed back to abc frame and normalized with respect to the DC link voltage to be used as reference signals to generate the inverter switches trigger pulses based on SPWM technique.

III. SIMULATION RESULTS

In order to validate the feasibility and the effectiveness of the proposed grid-connected centralized inverter topology, a numerical model of the entire system is simulated for 100 KW PV array farms of 320 modules by using Matlab/Simulinksoftware environment. The most important parameters of the system are given in Table I. For all simulations, the temperature is assumed constant at 25 ℃.

First of all, to demonstrate the effect of partial shading on the characteristics of PV array let us consider the following two scenarios. The first scenario is a conventional 10×32 series-parallel (SP) array with

bypass diodes every 5 series modules (i.e. 2×32 series-parallel strings). While in the second scenario, the PV array is stacked through 2×4 series-parallel CCOs (i.e. each H-bridge is connected to a substring of 5 series modules), which is equivalent to the first scenario. For both scenarios assume that 50% of substrings are illuminated by irradiation level of 0.6 kW/m² while the other 50 % are fully illuminated with irradiation level of 1 kW/m². Figure 6 shows the corresponding *P-V* characteristics of the two scenarios during partial shading and in case of clear sky (note: both scenarios have the same characteristics under clear sky condition). The output characteristics of PV array farm in both cases are obtained by sweeping the terminal voltage from 0 to array open circuit voltage that is 646 V.

As can be seen from figure 6, in case of conventional SP array with bypass diodes, the *P-V* characteristics exhibit multiple MPPs, involving a global MPP and local MPP, which increases the probability of false tracking of MPP and need to an advanced MPPT algorithm to track the global MPP. On the other hand, in the case of CCO, the *P-V* characteristics have a unique MPP which easy to follow by a simple MPPT algorithm. The maximum powers generated in case of clear sky, shaded CCO, and shaded SP array are 100 KW, 90 KW, and 81.5 KW at MPP voltages 547 V, 545 V, and 554 V respectively.
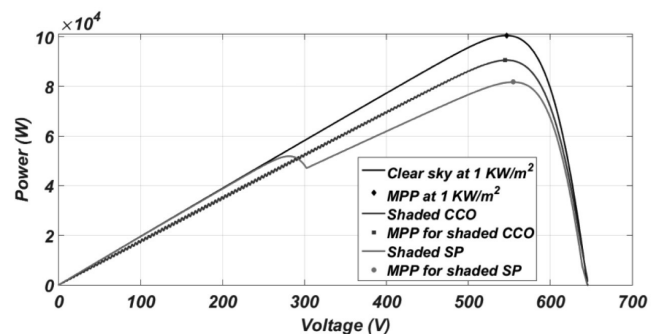
Figure 6 shows the *P-V* characteristics of the two scenarios during partial shading and clear sky
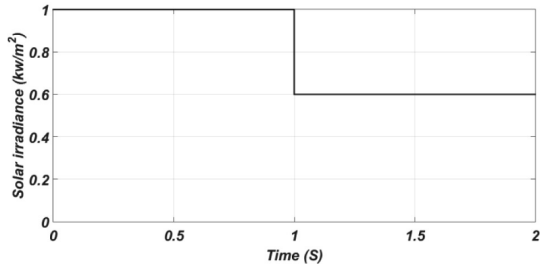
(a) The solar irradiance profile for 50% of substrings.
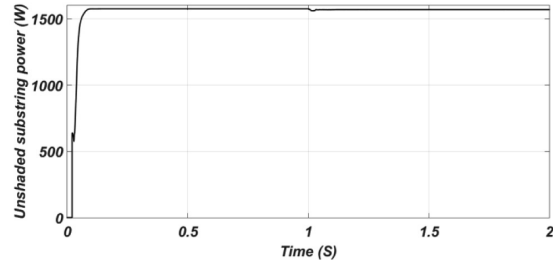
(b) The output power of unshaded substring.
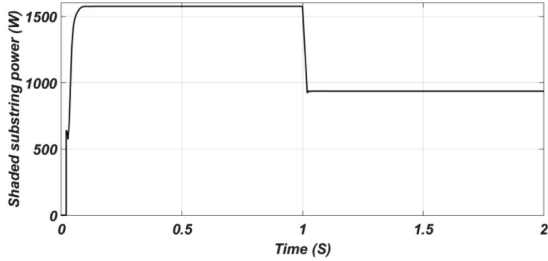
(C) The output power of unshaded substring.
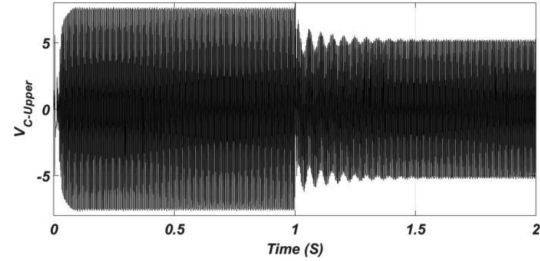
(d) The voltage across upper coupling condensers of CCOs.
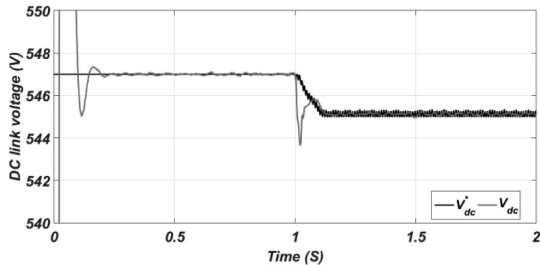
(e) The DC link capacitor voltage.
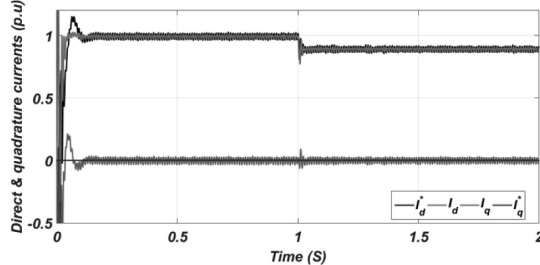
(f) The direct & quadrature current components.
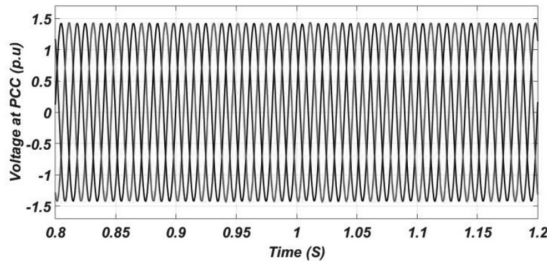
(g) The three phase grid voltage waveform at PCC.
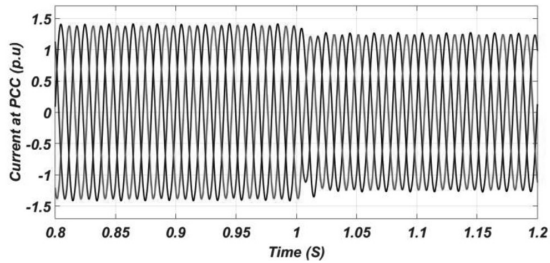
(h) The three phase grid current waveform at PCC.
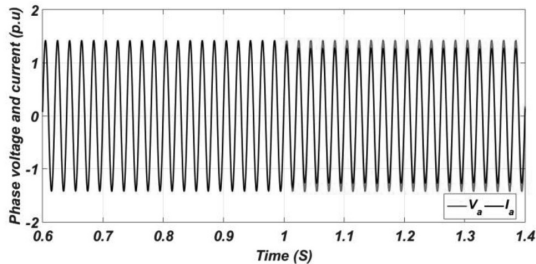
(i) Dynamic response of phase current and phase voltage.
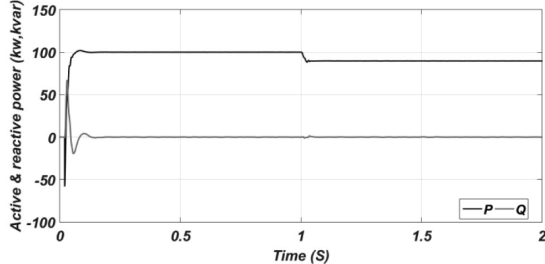
(j) The powers transferred to the grid at PCC.
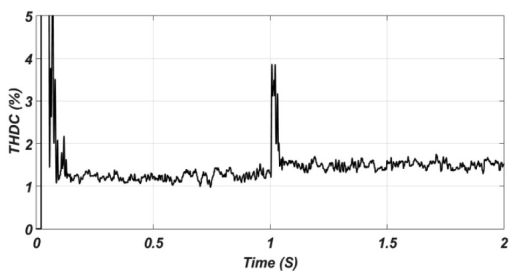
(k) The THD of current in time domain at PCC
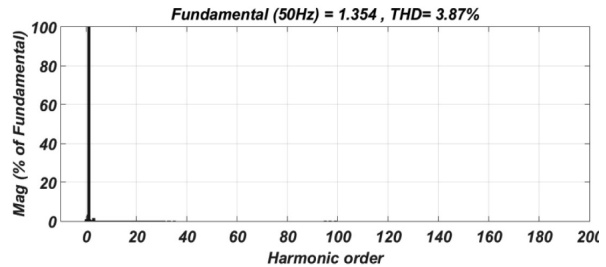
(l) The grid current spectrum at PCC.

Figure 7. Simulation results under transient condition

This means that 9,4% of expected power is lost in bypass diodes of conventional topologies in this shading situation.

In order to investigate the effectiveness of the controllers, a dynamic simulation is done with partial shadow discussed earlier for 50% of substrings as shown in figure 7(*a*). Simulation results under transient condition are shown in figure 7(*b*) through figure 7(*l*). Figures 7(*b, c*) show the output power of shaded and unshaded substrings during the simulation run. As can be seen, the irradiation level dropped at 1 second and has an immediate effect on the substring output power.

The voltage magnitude across coupling condensers of CCOs is dropped to compensate this situation of partial shading and collect the total power from shaded and unshaded substrings at approximately MMP voltage. The voltage across the upper condensers is as shown in figure 7(*d*), while the voltage across the lower condensers is out-of-phase with upper condensers.

The DC link voltage is monitored to verify the operation of the DC link controller and make sure it tracks the MPP voltage. As can be seen in figure 7(*e*), the DC link voltage kept tracking the MPP provided by *P&O* algorithm and decrease from 547 V to 545 V. This was expected where the P-V characteristics in figure (6) confirm this result. The *dq* components of the injected current are shown in figure 7(*f*). The direct component of the injected current is controlled to follow the new reference value dictated by the DC link controller at 0.9 p.u, which is dropped from 1 p.u in case of clear sky. The reference for the quadrature component, however, stayed at zero to maintain unity power factor operation. It is significant to note that, the response of controllers are suffered from some transients at the beginning of simulation as the PLL synchronized with grid voltage angle and due to charging of DC link capacitor.

The dynamic behaviors of three-phase grid voltage and grid current at PCC are shown in figure 7(*g, h*). As also expected, the grid voltage waveform does not change during the transient since it is set by the AC network, whereas the grid current amplitude decreases in response because of partial shadow. Fig. 7(*i*) illustrates the phase angle between phase current and phase voltage at PCC, where the grid current is in phase with the grid voltage (i.e. unity power factor).

The active and reactive powers transferred to the grid at PCC are shown in figure 7(*j*). The active power is initially at 100 kW before dropping to 90 KW after occurs of partial shading, while the reactive power injected into the grid is kept at zero Kvar. The total harmonic distortion of the current (THDC) at PCC in time domain as well as in frequency domain is shown in figure 7(*k, l*). As can be seen, the THD of the injected current does not exceed the 5% limit set by IEEE standard 929.

Parameters for simulation

PV module type	SPR-315E-WHT-D, SunPower
Module output power at MPP	315 W
Module output voltage at MPP	54,7 V
Module output current at MPP	5,76 A
Module open circuit voltage	64,6 V
Module short circuit current	6,14 A
CCO components	
Capacitance of coupling condensers	500 µF
Inductance of coupling transformers	5 mΩ
Resistance of coupling transformers	50 mH
Switching frequency of SCRs	340 Hz
Switching frequency of VSI	99×50 Hz
Capacitance of DC link capacitor	5000 µF
LC filter	
Filter inductance	500 µH
Filter capacitance	180 µF
Damping resitance	143 mΩ
PV interfacing transformer	
KVA rating	100 KVA
Transformation ratio	285V/6 KV
Per unit impedance	$(0,123 + j1,23)\%$
Grid voltage	6 KV
Grid frequency	50 Hz
Short circuit level	500 KVA
X/R ratio	7

IV. CONCLUSION

This paper proposed a new centralized inverter topology based on a novel CCO for application in DG system. The main targets were to improve the power harvest from PV array during partial shading condition, avoid the misleading power loss due to local MPPs, eliminate the power loss associated with circulating currents between parallel PV generators, and inject a high quality AC current into the grid to meet the standard IEEE 929. Simulation results on MATLAB/Simulink software environment have been carried out in order to confirm the proposed topology operation under partial shading conditions.

Simulation results show that the proposed topology offers an excellent steady-state response, fast dynamic response, low total harmonic current distortion, perfect and robust tracking of maximum power point during partial shading condition. Furthermore, the current injected into the grid was in phase with the grid voltage

(i.e. unity power factor). Therefore, the system performance met the standard IEEE 929.

According to results, the maximum power generated by using CCOs was significantly increased compared to conventional topology with SP array under partial shading pattern. In addition, local MPPs that found in case of SP approach were successfully eliminated by using the CCO circuit. Hence, the optimizer did not suffer from misleading power loss and only required a simple MPPT algorithm to follow the MPP. Moreover, the voltage difference between parallel PV generators; due to partial shading, PV modules mismatch, or PV modules aging were compensated through the optimizer to a current consolidation point. Therefore, the circulating currents between parallel PV generators were eliminated.

———————————REFERENCE———————————

1. **Bao C., Ruan X., Wang X., Li W., Pan D., Weng K.** Step-by-step controller design for LCL-Type Grid-Connected inverter with capacitor-current-feedback active-damping. — IEEE Trans. Power Electron., 2014, vol. 29, No. 3, pp. 1239—1253.

2. **Refaat A., Kalas A., Daoud A., Bendary F.** A Control Methodology of Three Phase Grid Connected PV System, in Clemson University Power Systems Conference, 2013.

3. **Hasan R., Mekhilef S., Seyedmahmoudian M., Horan B.** Grid-connected isolated PV microinverters: A review, Renew. Sustain. Energy Rev., 2017, vol. 67, pp. 1065—1080.

4. **Kandemir E., Cetin N.S., Borekci S.** A comprehensive overview of maximum power extraction methods for PV systems. — Renew. Sustain. Energy Rev., 2017, vol. 78, pp. 93—112.

5. **Uno M. and Kukita A.** Single-Switch Voltage Equalizer Using Multistacked Buck #x2013; Boost Converters for Partially Shaded Photovoltaic Modules. — IEEE Trans. Power Electron., 2015, vol. 30, No. 6, pp. 3091—3105.

6. **Nimni Y. and Shmilovitz D.** A returned energy architecture for improved photovoltaic systems efficiency. — 2010 IEEE International Symposium on Circuits and Systems: Nano-Bio Circuit Fabrics and Systems, 2010, pp. 2191—2194.

7. **Fernando L., Villa L., Ho T., Crebier J., Raison B.** A Power Electronics Equalizer Application for Partially Shaded Photovoltaic Modules. — IEEE Trans. Ind. Electron., 2013, vol. 60, No. 3, pp. 1179—1190,.

8. **Ben-Yaakov S., Blumenfeld A., Cervera A., Evzelman M.** Design and evaluation of a modular resonant switched capacitors equalizer for PV panels. — IEEE Energy Conversion Congress and Exposition. 2012, pp. 4129—4136.

9. **Bergveld H. J., Bьthker D., Castello C., Doorn T., Jong A. De., Van Otten R., De Waal K.** Module-level DC/DC conversion for photovoltaic systems: The delta-conversion concept. — IEEE Trans. Power Electron., 2013, vol. 28, No. 4, pp. 2005—2013.

10. **Giral R., Carrejo C.E., Vermeersh M., Saavedra-Montes A.J., Ramos-Paja C.A.** PV field distributed maximum power point tracking by means of an active bypass converter. — 3rd International Conf. on Clean Electrical Power, Renewable Energy Resources Impact, 2011, pp. 94—98.

11. **Qin S., Cady S.T., Dominguez-Garcia A.D., Pilawa-Podgurski R.C.N.** A distributed approach to MPPT for PV sub-module differential power processing. — IEEE Energy Conversion Congress and Exposition, 2013, pp. 2778—2785.

12. **Shenoy P.S., Kim K.A., Johnson B.B., Krein P.T.** Differential power processing for increased energy production and reliability of photovoltaic systems. — IEEE Trans. Power Electron., 2013, vol. 28, No. 6, pp. 2968—2979.

13. **Kadri R., Gaubert J.P., Champenois G.** New converter topology to improve performance of photovoltaic power generation system under shading conditions. — Intern. Conf. on Power Engineering, Energy and Electrical Drives, 2011, pp. 1—7.

14. **Giral R., Ramos-Paja C.A., Gonzalez D., Calvente J., Cid-Pastor A., Martinez-Salamero L**. Minimizing the effects of shadowing in a PV module by means of active voltage sharing. — Proceedings of the IEEE Intern. Conf. on Industrial Technology, 2010, pp. 943—948.

15. **Shimizu T., Hashimoto O., Kimura G**. A novel high-performance utility-interactive photovoltaic inverter system. — IEEE Trans. Power Electron., 2003, vol. 18, No. 2, pp. 704—711.

16. **Du J., Xu R., Chen X., Li Y., Wu J.** A novel solar panel optimizer with self-compensation for partial shadow condition. — IEEE Applied Power Electronics Conference and Exposition, 2013, pp. 92—96.

17. **IEEE Recommended** Practice for Utility Interface of Photovoltaic (PV) Systems. — IEEE Std 929-2000, 2000, p. 26.

18. **Refaat A., Kalas A., Daoud A., Bendary F.** A Control Methodology of Grid-Connected PV System to Verify The Standard IEEE 929-2000. — Proceedings of the 15th Intern. Middel East Power System Conf. (MEPCON?12), 2012.

19. **USSR patent, N 738044,** H 02 J 1/10, 1976. Loading system of a multi-electrode magnetohydrodynamic generator / B.M. Antonov, V.A. Labuntzov, V.V. Laskin, A.T. Sultanov..

20. **Liserre M., Blaabjerg F., Hansen S.** Design and Control of An LCL-Filter Based Three-Phase Active Rectifier. — IEEE Trans. Ind. Appl., 2005, vol. 1, No. 5, pp. 1281—1291.

21. **Dannehl J., Wessels C., Fuchs F.W.** Limitations of Voltage-Oriented PI Current Control of Grid-Connected PWM Rectifiers With Filter. — IEEE Trans. Ind. Electron., 2009, vol. 56, No. 2, pp. 380—388.

A u t h o r s: **Refaat A.** — *Electrical Power Engineering Department, Port Said University, Egypt*

Elgamal M. — *Electrical Power Engineering Department, Mansoura University, Egypt*

Korovkin N.V. — *Theoretical Electrical Engineering and Electromechanics Department, Peter the Great Saint-Petersburg Polytechnic University, Saint-Petersburg, Russia*

Новая централизованная топология фотоэлектрических преобразователей, работающих с сетью, оптимизированная для условий частичного затенения

РЕФААТ А., ЭЛГАМАЛ М., КОРОВКИН Н.В.

Централизованные инверторы с сетевым подключением, основанные на традиционных тополо-гиях — одно из лучших решений для средних и крупных фотоэлектрических электростанций благо-

даря их низкой стоимости и простоте. Однако выходная мощность этих традиционных решений резко снижается из-за эффектов частичного затенения панелей и(или) при разбросе параметров фотоэлектрических панелей. В статье предлагается новая топология централизованного инвертора, подключенного к сети, основанная на сумматоре тока, которая повышает выходную мощность фотоэлектрической матрицы в случае ее частичного затенения или несовпадения параметров фотоэлектрических модулей. Фотоэлектрические модули устанавливаются в стек сумматора, а затем подключаются к сети через трехфазный инвертор напряжения. Сумматор используются для улучшения сбора энергии от фотоэлектрической матрицы вместо обходных и блокирующих диодов, которые искажают характеристики фотоэлектрической матрицы и уменьшают ее выходную мощность. Инвертор напряжения применяется для подачи высококачественного переменного тока в сеть и совместного отслеживания режима максимальной мощности. Для проверки работы предложенной топологии выполнено компьютерное моделирование с использованием MATLAB/Simulink. Результаты моделирования показывают, что предложенная топология обеспечивает хороший отклик в устойчивом состоянии, быстрый динамический отклик, совершенное и надежное отслеживание точки максимальной мощности в условиях частичного затенения.

К л ю ч е в ы е   с л о в а: *фотогальваническая система, оптимизация суммирования токов, централизованные инверторы, подключение к сети, управляемый инвертор напряжения, отслеживание максимальной мощности, качество электроэнергии, эффективность, частичное затенение*

А в т о р ы: **Рефаат А.** − *Электроэнергетический департамент университета, Порт-Саид, Египет*

Элгамал М. − *Электроэнергетический департамент университета, Мансоура, Египет*

Коровкин Н.В. − *Институт теоретической электротехники и электромеханики Санкт-Петербургского политехнического университета Петра Великого, Россия*